minerals

MDPI

Article

Long-Lasting Magmatic, Metamorphic Events in the Cathaysia Block: Insights from the Geochronology and Geochemistry of Inherited Zircons in Jurassic A-Type Granites

Wenzhou Xiao [1,*], Feng Zi [2], Chenguang Zhang [3], Fenquan Xie [4], Ioan V. Sanislav [5], Mohammed S. Fnais [6] and Mabrouk Sami [7,8,*]

[1] Hunan Key Laboratory of Rare Metal Minerals Exploitation and Geological Disposal of Wastes, School of Resource Environment and Safety Engineering, University of South China, Hengyang 421001, China
[2] School of Earth Sciences and Spatial Engineering, Hunan University of Science and Technology, Xiangtan 411201, China; zifeng@hnust.edu.cn
[3] School of Geographic Sciences, Xinyang Normal University, Xinyang 464099, China; paladin@xynu.edu.cn
[4] Bohai-Rim Energy Research Institute, Northeast Petroleum University, Qinhuangdao 066000, China; xfqyongyuan@126.com
[5] Economic Geology Research Centre (EGRU), College of Science and Engineering, James Cook University, Townsville, QLD 4811, Australia; ioan.sanislav@jcu.edu.au
[6] Department of Geology and Geophysics, College of Science, King Saud University, Riyadh 11451, Saudi Arabia; mfnais@ksu.edu.sa
[7] Geosciences Department, College of Science, United Arab Emirates University, Al Ain 15551, United Arab Emirates
[8] Geology Department, Faculty of Science, Minia University, El-Minia 61519, Egypt
* Correspondence: lilzhou@usc.edu.cn (W.X.); mabrouksami@uaeu.ac.ae (M.S.)

Abstract: The Paleoproterozoic basement underlying the Cathaysia Block remains relatively understudied, and its contribution to the region's tectonic evolution requires further investigation. In this study, we examined Jurassic Laiziling and Jianfengling A-type granites and identified a significant number of zircon grains exhibiting varied CL imaging characteristics. These zircons yielded four distinct age groups: <100 Ma, 200–100 Ma, 500–200 Ma, and >700 Ma. Detailed trace element analysis revealed that these age groups correspond to different zircon types: metamorphic recrystallized zircons (<100 Ma), primary magmatic zircons (200–100 Ma), and inherited zircons (500–200 Ma and >700 Ma). Through host rock and tectonic setting discrimination, we consider that the inherited zircons have host rocks of S-type granites and basic rocks, and these were formed in subduction-compression tectonic environments. In comparison to local significant geological events in history, we propose that these zircons record multiple tectonic events in the South China Block, including the amalgamation of the Yangtze and Cathaysia Blocks during the Neoproterozoic; an intracontinental orogenic event that occurred during the Middle Paleozoic; and subduction–exhumation processes related to the Paleo-Pacific slab; as well as extensional metamorphic events from the Cretaceous to Tertiary events. A comparison of Hf isotopic compositions revealed that zircons aged 500–200 Ma and >700 Ma share a 2.5–1.6 Ga crustal evolution zone, indicating that multiple re-melting events have occurred within the Paleoproterozoic basement of the Cathaysia Block.

Keywords: paleoproterzoic basement; caythsia block; inherited zircon; re-melting event

Citation: Xiao, W.; Zi, F.; Zhang, C.; Xie, F.; Sanislav, I.V.; Fnais, M.S.; Sami, M. Long Lasting Magmatic, Metamorphic Events in the Cathaysia Block: Insights from the Geochronology and Geochemistry of Inherited Zircons in Jurassic A-Type Granites. *Minerals* **2024**, *14*, 1247. https://doi.org/10.3390/min14121247

Academic Editor: Constantin Athanassas

Received: 10 October 2024
Revised: 29 November 2024
Accepted: 5 December 2024
Published: 7 December 2024

1. Introduction

The Cathaysia Block, typically regarded as the southeastern portion of the South China Block, is considered relatively young due to its limited exposure of ancient strata [1–3]. The Yangtze and Cathaysia Blocks amalgamated along the Jiangnan Orogenic Belt during the Neoproterzoic, leading to the formation of the present-day South China Block

[2,4,5]. In contrast to the Northwestern Yangtze Block, which possesses an Archean basement [2,6], the oldest strata discovered in the Cathaysia Block are Neoproterzoic in age [7]. Moreover, the Cathaysia Block exhibits minimal Proterzoic magmatism activity, with the exception of the Badu complex, which is a unique assemblage of Paleoproterzoic S- and A-type granites with ages of 1.9–1.8 Ga [8–10]. However, no Proterzoic magmatic rocks were found in the remaining area of the Cathaysia Block. This scarcity of Proterzoic magmatic rocks and strata has resulted in an incomplete understanding of the Cathaysia Block's formation and tectonic evolution.

Recent studies have revealed the occurrence of numerous detrital and inherited zircons in post-Proterzoic rocks, exhibiting unusually old ages of the Paleoproterzoic or even the Archean rocks, suggesting the existence of an underlying older basement [9,11–13]. Many studies have reported the new viewpoint that an unexposed Archean basement does exist underneath the Cathaysia Block [11,12,14]. However, the largest number of detrital zircons found within the strata display Hf isotopic compositions that correspond to a 1.6–2.5 Ga crustal growth zone [15]. This indicates a major geological event during the Paleoproterozoic Era that contributed to the formation of an underlying basement. Nevertheless, there has been limited research focusing on the subsequent remelting events affecting the Paleoproterozoic basement, and its role in influencing the tectonic evolution of the Cathaysia Block remains poorly understood.

The Xianghualing intrusions, comprising two granitic stocks, represent typical A-type granites exposed in the Nanling Range of the Cathaysia Block [16]. Similar to many highly evolved granites in this region, the Xianghualing intrusions contain a significant number of inherited zircons, which is attributed to their relatively low crystallization temperature [12]. In this study, we conducted comprehensive analyses of U-Pb ages, Hf isotopes, and trace elements of these captured zircons to elucidate their host rocks, formation mechanisms, and geological backgrounds. Our objective was to clarify the contribution of the Paleoproterozoic basement to the subsequent tectonic events and reconstruct a detailed tectonic evolution of the Cathaysia Block.

2. Geological Background and Sample Description

The Cathaysia Block is situated in the southeastern part of the South China Block (Figure 1a) and is thought to have amalgamated with the Yangtze Block along the Jiangnan Orogenic Belt during the Neoproterzoic Era, resulting in the formation of the South China Block [2,4,5,17]. In contrast to the Yangtze Block, which is characterized by multiple exposed Archean rocks and can be classified as a craton [2,6], the Cathaysia Block lacks exposed Archean rocks and is usually regarded as an accretionary block [2,3].

The Nanling Range, located in the southwestern part of the Cathaysia Block (Figure 1a), exhibits a relatively complete stratigraphic sequence ranging from the Proterozoic to the Jurassic Eras, with the exception of the Silurian Era [18]. The oldest strata in this range are the Mesoproterzoic Lengjiaxi Group and the Neoproterozic Banxi Group, composed primarily of metamorphosed slate and sandstone. The overlying Sinian and Cambrian sequences consist mainly of slate, sandstone, limestone, and dolomite. The Ordovician strata are predominantly composed of limestone, which is overlain by Devonian and Carboniferous carbonate rocks, which are the most widely developed strata in this area. The Permian and Triassic strata mainly consist of limestone, dolomite, and shale, while the Jurassic and Cretaceous strata are less widespread, and are mainly composed of sandstones.

The Xianghualing area, located at the northwestern margin of the Cathaysia Block and adjacent to the Jiangnan Orogenic Belt (Figure 1a,b), hosts four small granitic intrusions and four felsic dikes (Figure 1c). Among these, the northernmost Laiziling granitic stock and the southernmost Jianfengling granitic stock are the largest intrusions and are recognized as the primary ore-bearing granites in the region. Previous studies have identified the Laiziling and Jianfengling stocks as being highly evolved A-type granites, with ages of 156–150 Ma and 165–160 Ma, respectively [16]. Both granitic stocks exhibit vertical

zonation with distinct lithologies: biotite granite at the base, zinnwaldite granite in the middle, and topaz granite at the top [12,19,20].

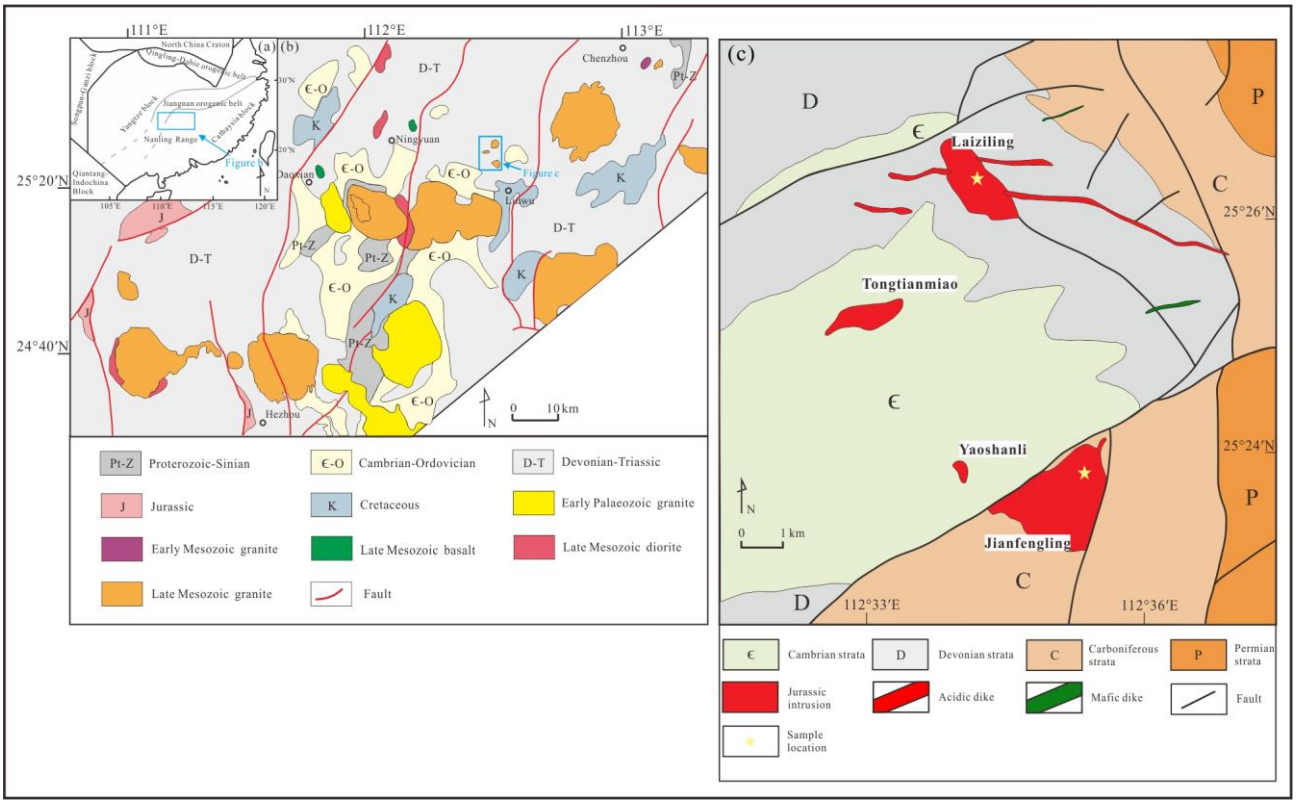

Figure 1. (**a**) A tectonic map of the South China Block; (**b**) a geological map of the Nanling Range; and (**c**) a geological map of the Xianghualing area.

In this study, fine-grained zinnwaldite granites were collected from hillside exposures in the Xianghualing area for zircon picking and analysis; collected sample coordinates are presented in Supplementary Table S1. The Laiziling granites are light gray to whitish, massive, and fine-grained (0.5–2 mm) (Figure 2a,c), and are composed of quartz (35%–40%), plagioclase (20%–25%), K-feldspar (25%–30%), and muscovite (~5%), with accessory zircon, apatite, monazite, and ilmenite (Figure 2e). Similarly, the Jianfengling granites are also fine-grained (0.5–2 mm) (Figure 2b,d), massive, and of a light gray to whitish colored, consisting of quartz (35%–40%), plagioclase (15%–20%), K-feldspar (30%–35%), and muscovite (~5%), with accessory apatite, monozite, and ilmenite (Figure 2f).

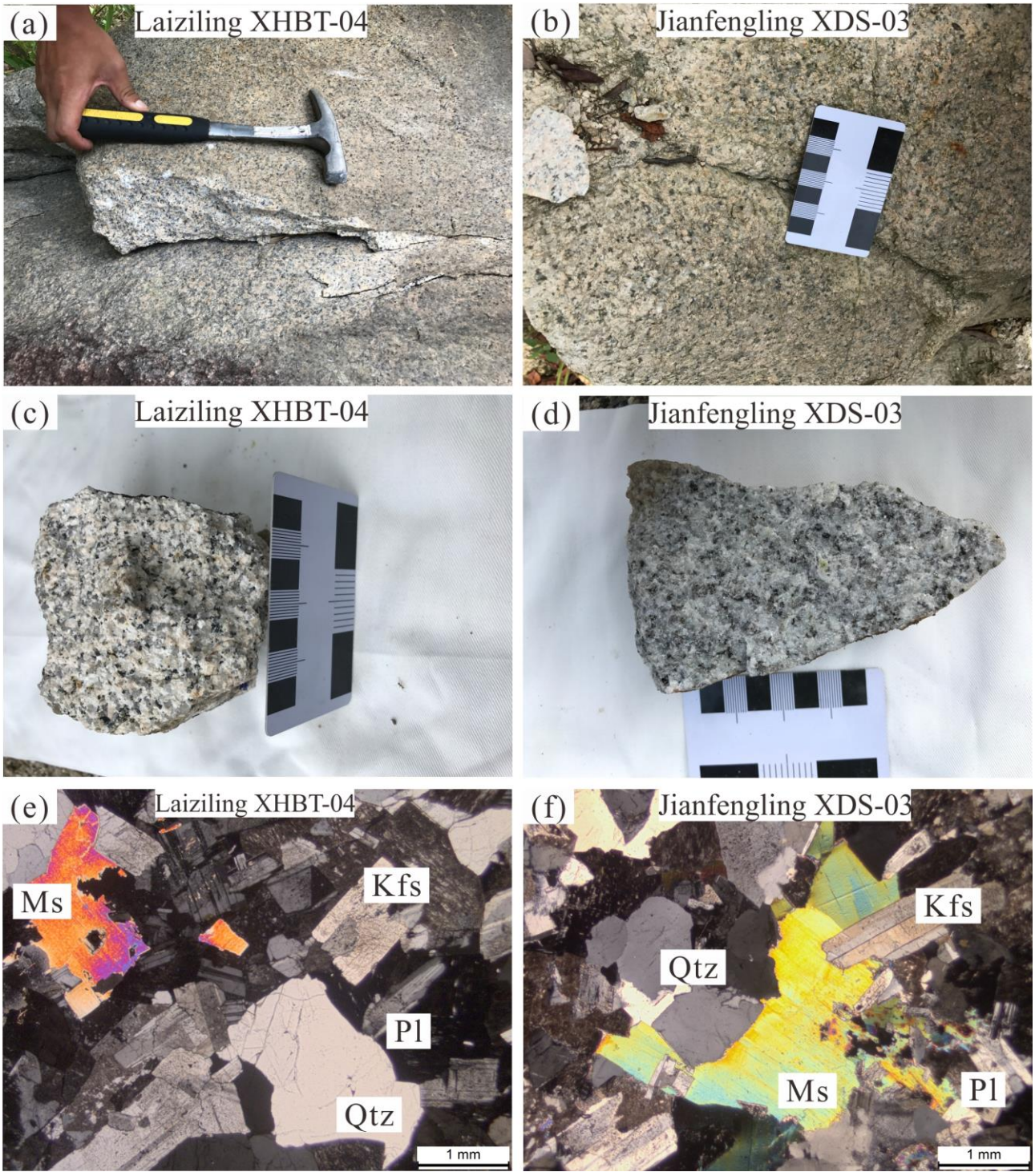

Figure 2. (**a**) Field outcrop photo of the Laiziling granite**;** (**b**) Field outcrop photo of the Jianfengling granite**;** (**c**) A hand specimen photo of the Laiziling granite; (**d**) a hand specimen photo of the Jianfengling granite; (**e**) a photomicrograph of the Laiziling granite; and (**f**) a photomicrograph of the Jianfengling granite. Images (**c**,**d**) are under cross-polarized light. Abbreviations: Kfs—K-feldspar; Ms—muscovite; Pl—plagioclase; Qtz—quartz.

3. Analytical Methods

3.1. Zircon U-Pb Dating and Trace-Element Analysis

Zircon grains were separated from the Laiziling and Jianfengling granites using standard magnetic and heavy liquid separation techniques at Langfang Integrity Geological Services Co., Ltd. (Langfang, China) Zircon grains were then carefully selected under

a binocular microscope to ensure purity. The selected zircon grains were embedded in epoxy resin blocks and polished to create flat surfaces for subsequent analysis.

Cathodoluminescence (CL) imaging was performed using a scanning electron microscope (SEM) at Chongqing Yujing Science and Technology Services Co., Ltd., (Chongqing, China) to reveal the internal structures of the zircon grains. Zircon U-Pb geochronology and trace element analysis were carried out via laser ablation inductively coupled plasma-mass spectrometry (LA-ICP-MS) at Nanjing FocuMS Technology Co., Ltd. (Nangjing, China) The experimental setup employed a Teledyne Cetac Technologies Analyte Excite LA system (Bozeman, MT, USA) combined with an Agilent Technologies 7700× quadrupole ICP-MS (Hachioji, Japan). Ablation was performed using a 193 nm ArF excimer laser, homogenized by a set of beam delivery systems, and was focused on the zircon surfaces at a fluence of 6.0 J cm^{-2} with a spot diameter of 35 μm and an 8 Hz repetition rate for 40 s, resulting in 320 laser pulses. Helium was used as the carrier gas to transport the ablated material to the ICP-MS.

Zircon 91,500 served as the external reference material for U-Pb age correction, and GJ-1 was used for quality control during geochronological analysis. Lead and other trace elements concentrations were calibrated externally against NIST SRM 610, with Si serving as the internal standard following the methodologies of [21,22]. Data reduction was performed using the ICPMSDataCal 11 software [21,23]. Quantitative calibration for Pb isotope dating was performed by ComPbcorr#3_18 [24]. Concordia diagrams and weighted mean age calculations were created using ISOPLOT 4.15 [25].

3.2. Zircon Hf Isotope Analysis

The Hafnium isotopic ratios of the zircon grains were measured using LA-MC-ICP-MS at Nanjing FocuMS Technology Co. Ltd., Nanjing, China. The Teledyne Cetac Technologies Analyte Excite laser-ablation system (Bozeman, MT, USA) was coupled with a Nu Instruments Nu Plasma II MC-ICP-MS (Wrexham, Wales, UK). A 193 nm ArF excimer laser, was homogenized by a set of beam delivery systems and was focused on the zircon surface with a fluence of 6.0 J/cm^2. Ablation occurred with a spot diameter of 50 μm at an 8 Hz repetition rate for 40 s (320 pulses). Helium was used as the carrier gas to efficiently transport the aerosol for MC-ICP-MS. Two zircon standards, GJ-1 and 91,500 [21,22], were analyzed alongside the samples for every ten unknown zircon grains to ensure quality control and accurate isotopic measurements.

4. Analytical Results

4.1. Zircon U-Pb Dating

The zircon U-Pb dating results are presented in Supplementary Table S2, and their representative CL images are in Figure 3, with concordant ages determined for 100 zircon grains. The majority of zircons yielded ages around 160 Ma (Figure 4). Numerous inherited zircons with dates older than 160 Ma were also identified, along with several younger zircons. The zircons span a date range from 2502 Ma and 34 Ma.

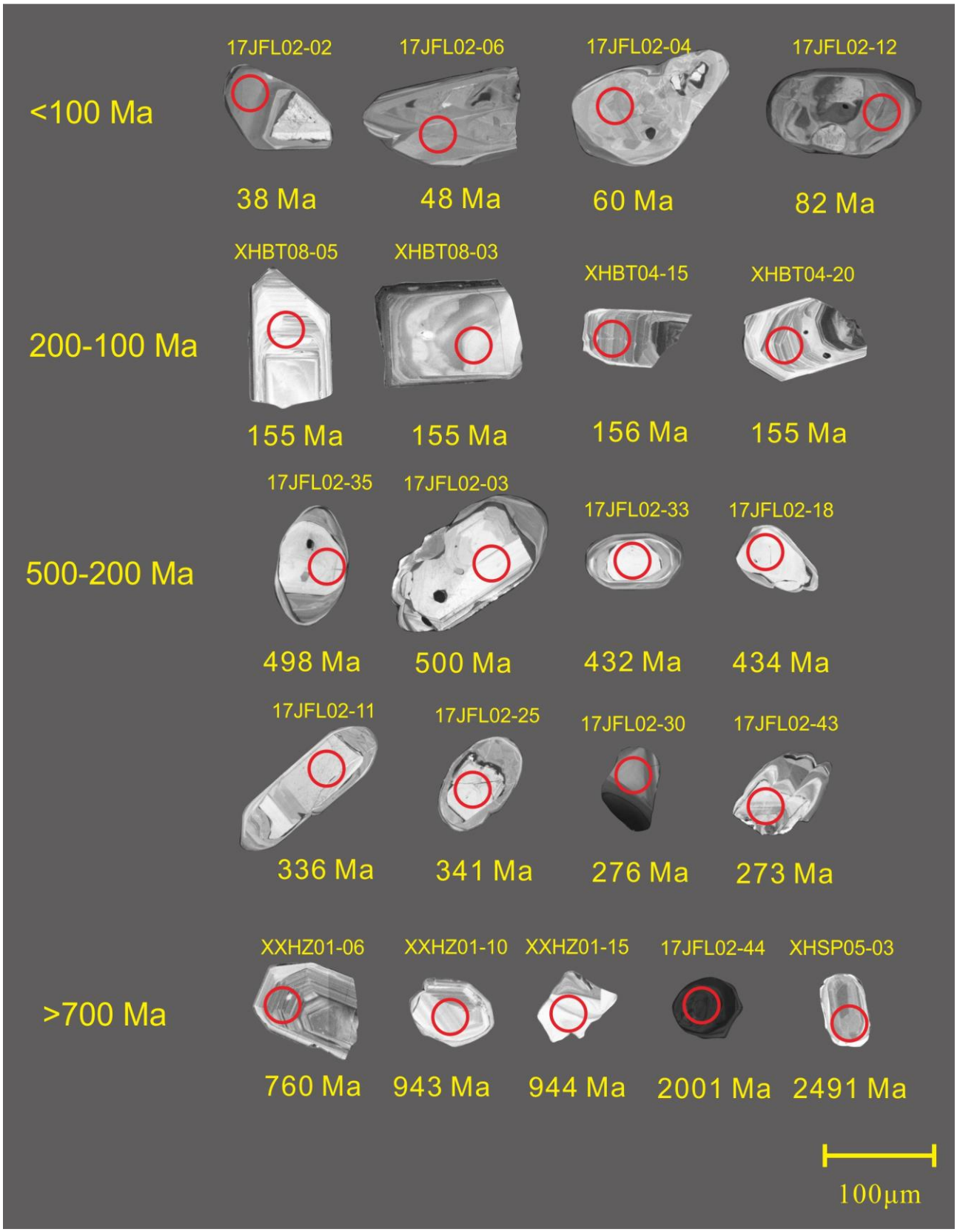

Figure 3. Representative zircon cathodoluminescence (CL) images.

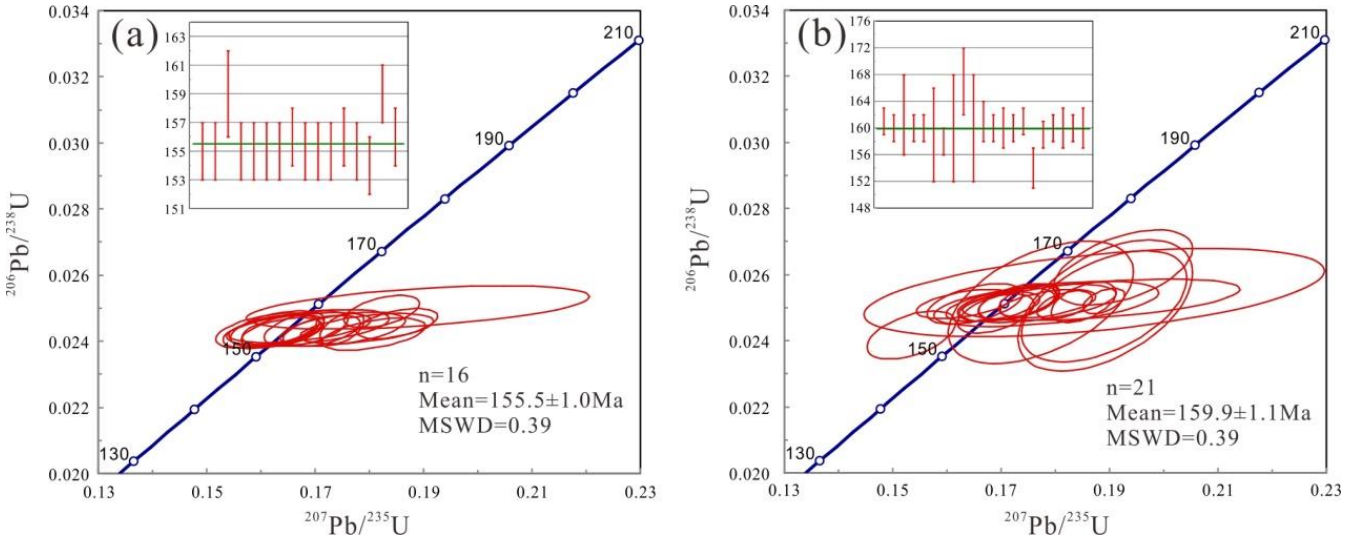

Figure 4. (**a**) U–Pb concordia diagrams and weighted mean $^{206}Pb/^{238}U$ age diagrams of zircons from (**a**) the Laiziling granites; and (**b**) the Jianfengling granites.

Zircons younger than 100 Ma typically formed as growth rims around zircons dated between 500 and 200 Ma, but also could be isolated grains. The isolated grains have well-defined grain sizes of 50–150 μm with length-to-width ratios of 1:1 to 3:1 and show planar or fan-like zoning rather than oscillatory zoning. Twelve concordant $^{206}Pb/^{238}U$ dates range from 92 Ma to 34 Ma, clustering the zircons into three groups around 90 Ma, 55 Ma, and 40 Ma (Figure 5a).

The zircons dated between 200 to 100 Ma have grain sizes of 50–150 μm and length-to-width ratios of 1:1 to 3:1. These zircons exhibit bright CL images and clear oscillatory zoning, or slightly darker CL images with oscillatory zoning. Forty-one spots yielded concordant $^{206}Pb/^{238}U$ dates of 186 Ma to 124 Ma, and thirty-nine among them clustered around 160 Ma (Figure 5b).

Zircons dated between 500 and 200 Ma often appear as cores surrounded by zircons younger than 100 Ma, and they also can be isolated grains. These zircons exhibit bright CL images without oscillatory zoning. These zircons have brighter CL images than zircons younger than 100 Ma and also show planar zonation without oscillatory zoning. Thirty-five spots yielded concordant $^{206}Pb/^{238}U$ dates ranging from 503 Ma to 272 Ma, with notable four groups at 500 Ma, 450 Ma, 350 Ma, and 270 Ma (Figure 5c).

Zircons older than 700 Ma, with grain sizes of 100–150 μm and length-to-width ratios of 1:1 to 3:1, predominantly exhibit bright CL images with oscillatory zoning, though some show darker CL images with similar zoning. Twelve concordant dates were identified, with zircons younger than 1000 Ma yielding ages between 977 Ma and 760 Ma, while those older than 1000 Ma show $^{207}Pb/^{206}Pb$ dates ranging from 2500 Ma to 1820 Ma, clustering around 950 Ma (Figure 5d).

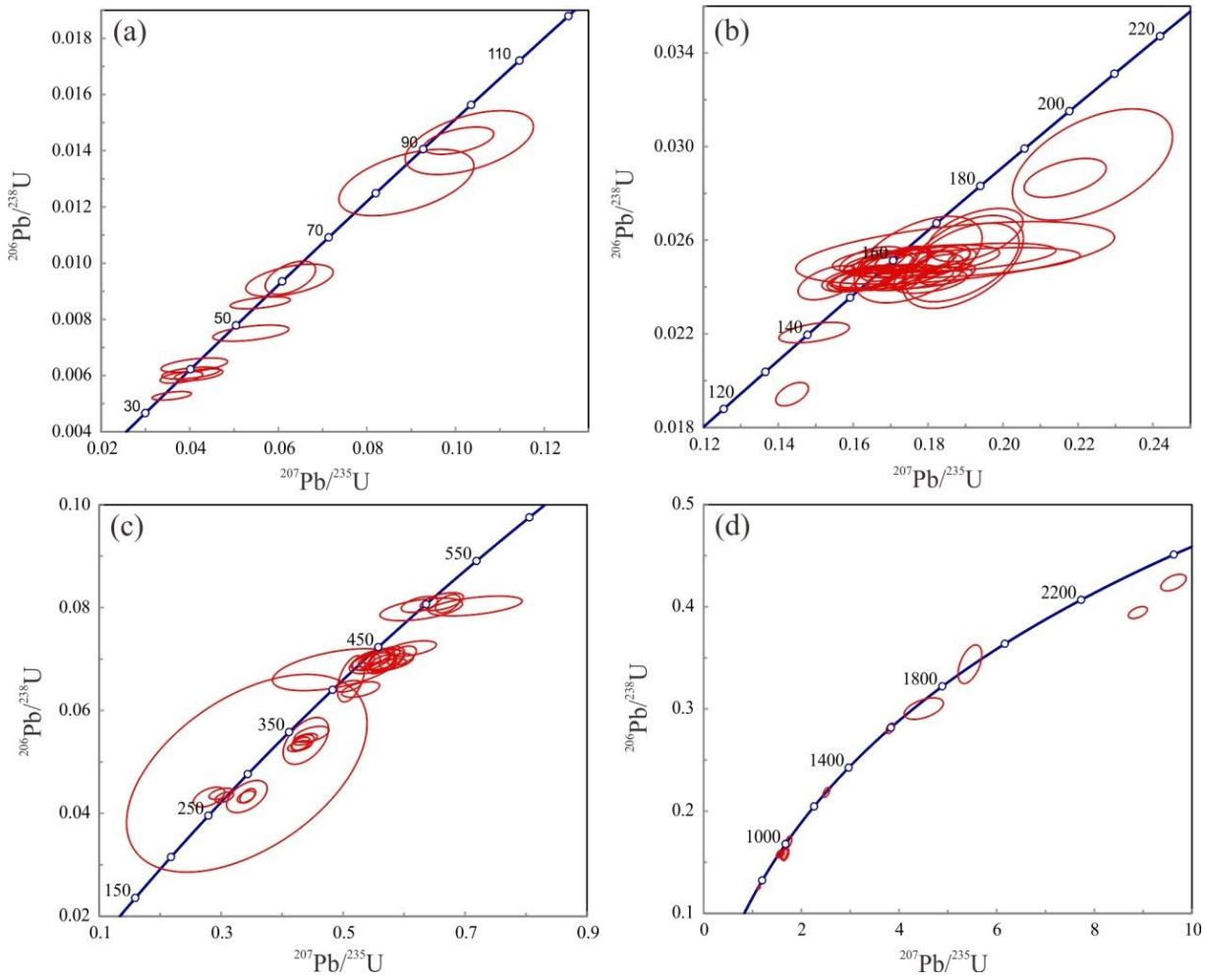

Figure 5. U–Pb concordia diagrams of zircons with (**a**) ages less than 100 Ma; (**b**) ages between 200 to 100 Ma; (**c**) ages between 500 to 200 Ma; and (**d**) ages greater than 700 Ma.

4.2. Zircon Morphology

Zircons from the Laiziling and Jianfengling granites display distinct morphological types accompanied with their age groups. Their sizes range between 50 and 150 μm. Zircons dated between 500 and 200 Ma exhibit extremely bright cathodoluminescence (CL) images without clear oscillatory zoning. These are often found as the cores of single zircon grains surrounded by dark growth rims, though they can also appear as single grains without growth rims. Zircons younger than 100 Ma show relatively bright CL images without oscillatory zoning and commonly form growth rims surrounding Zircons dates between 500 and 200 Ma. Occasionally, they also appear as single grains. The remaining zircon spot dates of 200–100 Ma and >700 Ma show either relatively bright CL images with significant oscillatory zoning and generally occur as individual grains, or are characterized by relatively dark CL images with oscillatory zoning and occur as single grains.

4.3. Zircon Trace Elements

The analytical results of zircon trace elements are provided in Supplementary Table S3. Zircons from the Laiziling and Jianfengling granites exhibit variable concentrations of Nb, Ta, Ti, Hf, Y, P, Th, and U, and their Th/U ratios and REE distribution patterns differ across age groups.

Zircons younger than 100 Ma show extremely low Th/U ranging from 0.01 to 0.42 except for one spot (average = 0.1 when excluding the spots with 1.46). These zircons exhibit low LREE contents, high HREE contents, distinct positive Ce anomalies (Ce/Ce* =

1.07–174.05), and slight negative Eu anomalies (Eu/Eu* = 0.40–0.96) in chondrite-normalized REE patterns (Figure 6a).

Zircons aged between 200 and 100 Ma have Th/U ratios ranging from 0.21 to 1.16 (average: 0.53). These zircons also show low LREE contents and high HREE contents, with distinct positive Ce anomalies (Ce/Ce* = 1.19–577.24) and negative Eu anomalies (Eu/Eu* = 0.003–0.49). Some zircons show elevated LREE contents (Figure 6b).

Zircons aged between 500 and 200 Ma exhibit Th/U ratios ranging from 0.25 to 1.88 (average: 0.91). Their REE patterns are characterized by low LREE contents, high HREE contents, positive Ce anomalies (Ce/Ce* = 1.68–441.26), and moderate negative Eu anomalies (Eu/Eu* = 0.09–0.57) (Figure 6c).

Zircons older than 700 Ma have Th/U ratios ranging from 0.17 to 1.44 (average: 0.65). In REE distribution diagrams, they exhibit low LREE contents, high HREE contents, positive Ce anomalies (Ce/Ce* = 1.06–105.89), and negative Eu anomalies (Eu/Eu* = 0.02–0.49). Several of these zircons show higher LREE contents (Figure 6d).

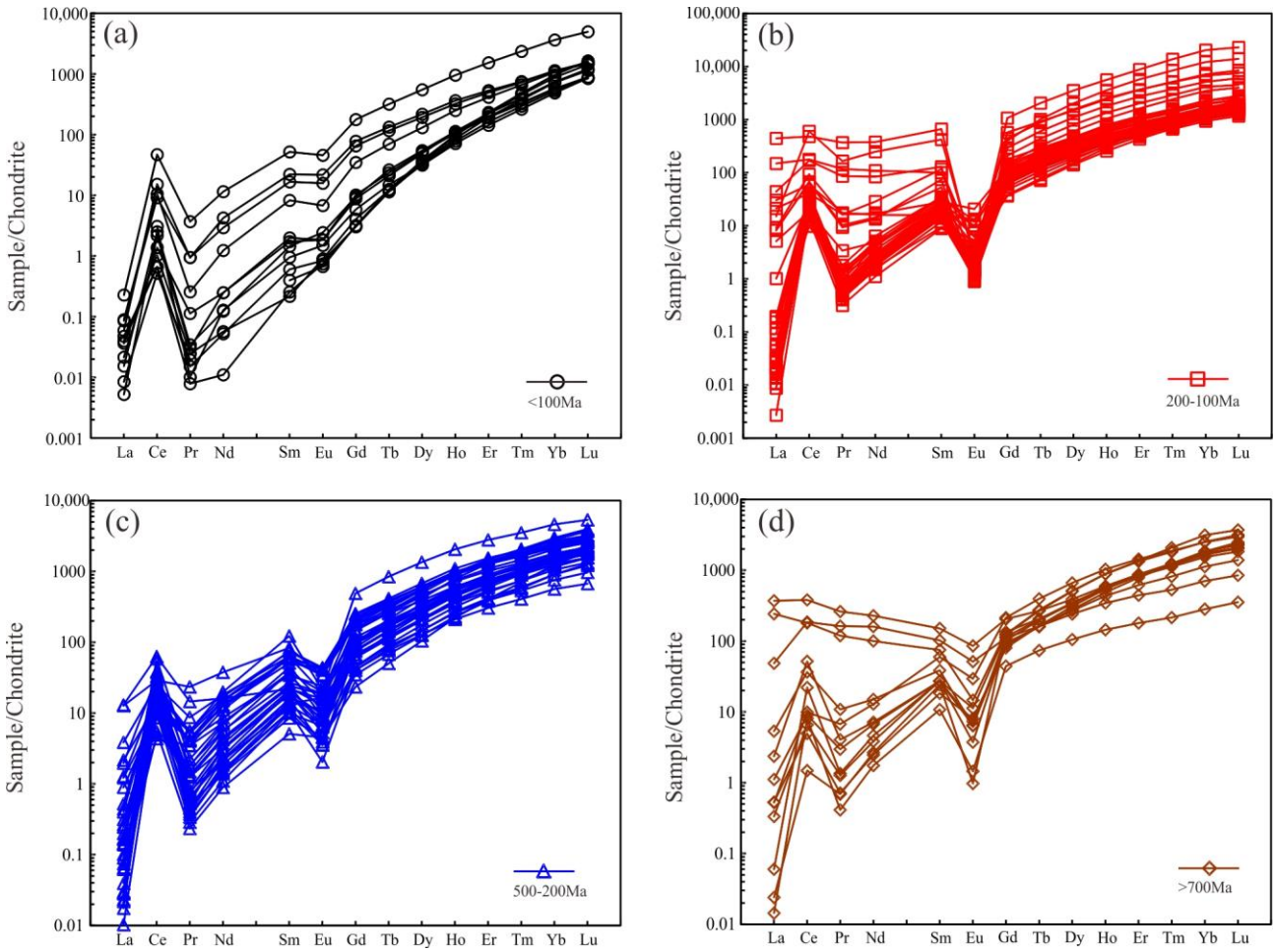

Figure 6. Chondrite-normalized rare earth element distribution pattern diagrams of zircons with (**a**) ages less than 100 Ma; (**b**) ages between 100 to 200 Ma; (**c**) ages between 200 to 500 Ma; and (**d**) ages greater than 700 Ma. The chondrite-normalized values are from [26].

4.4. Zircon Hf Isotope

The analytical results of zircon Hf isotopes are provided in Supplementary Table S4. Zircons younger than 100 Ma exhibit εHf(t) values ranging from −20.4 to −1.1 (average: −16.4), with two-stage model ages (T_{DM2}) ranging from 2424 to 1194 Ma (average: 2155 Ma). Zircons aged between 200 to 100 Ma show εHf(t) values between −22.8 to −2.7 (average: −7.0), with T_{DM2} ages ranging from 2633 to 1370 Ma (average: 1647 Ma). Zircons aged 500 to 200 Ma exhibit εHf(t) values between −17.3 and 9.5 (average: −11.6), with T_{DM2} ages

ranging from 2420 to 686 Ma (average: 2109 Ma). Zircons older than 700 Ma have εHf(t) values between −13.7 and 3.1 (average: −5.3), with T_{DM2} ages ranging from 2800 to 2513 Ma (average: 2522 Ma).

5. Discussion

5.1. Zircon Genesis: Magmatic, Metamorphic, or Hydrothermal?

Zircon morphology is a crucial indicator of crystallization environments, as zircons formed under different geological processes often exhibit distinct internal morphologies and structures. In acidic or intermediate magmatic rocks, zircons typically have larger grain sizes and well-developed oscillatory zoning [27]. Conversely, zircons crystallized in basic magmatic rocks are generally smaller with narrower grains, and may lack oscillatory zoning [27]. Hydrothermal zircons usually display good oscillatory zoning, but those that have undergone recrystallization or alteration by hydrothermal fluids often develop skeletal or spongy structures and contain numerous mineral inclusions [27–30]. Metamorphic zircons tend to exhibit more complex morphologies, depending on the specific metamorphic processes involved [27,31,32].

In addition, in the case of a zircon with a core–rim structure with wide differences in its core and rim, the core and rim usually represent two geological processes that are completely different [33–35]. In this study, zircons with ages <100 Ma and 500–200 Ma commonly occur as core–rim structures (rim domains with ages <100 Ma and core domains with ages of 500–200 Ma), with the core and rim exhibiting significant differences. These zircons display bright CL images but lack oscillatory zoning, showing instead planar or fan-like zonation. The rims are generally darker than the cores in CL images, suggesting two distinct geological events separated by a considerable time gap. However, zircon morphology alone cannot definitively differentiate magmatic from metamorphic origins. In contrast, zircons aged 200–100 Ma and >700 Ma exhibit clear oscillatory zoning and bright CL images, typical of zircons crystallized from magma. A few zircons with darker CL images retain oscillatory zoning, suggesting magmatic origin but with less metamictimation.

Trace element analysis provides additional insights into zircon crystallization environments. Hydrothermal zircons typically have higher overall REE contents than magmatic zircons, with elevated LREE levels and lower Ce-positive anomalies due to the presence of mineral or fluid inclusions rich in LREEs [15,28,36]. Discrimination diagrams such as $(Sm/La)_N$ vs. Ce/Ce* and La vs. $(Sm/La)_N$ are useful for distinguishing hydrothermal from magmatic zircons [37]. In this study, a small subset of zircons from the 200–100 Ma, 500–200 Ma, and >700 Ma age groups plot in the hydrothermal field (Figure 7a,b), characterized by high LREE contents and low Ce anomalies, and often display dark CL images indicative of metamictization or fluid alteration. Most other zircons, however, fall within the magmatic field, indicating that they crystallized from magma without significant alteration.

Distinguishing magmatic from metamorphic zircons can be challenging based solely on morphology, as metamorphism is a complex process involving various types [36,38]. However, differences in trace element compositions can help identify metamorphic zircons. Generally, metamorphic zircons exhibit lower Th/U ratios than magmatic zircons due to several mechanisms: (1) metamorphic fluids are typically enriched in U but deplete in Th [39,40], (2) zircon crystallization associated with Th-rich minerals leads to lower Th/U ratios [41,42], (3) during accretionary growth, U more easily enters the zircon lattice than Th [43], and (4) during metamorphic recrystallization, Th is preferentially expelled due to its larger ionic radius compared to U [36,44]. Metamorphic recrystallized zircons also tend to show positively correlated Th/U ratios and U-Pb ages, as radiogenic Pb is expelled during recrystallization, leading to younger U-Pb ages [44–46].

In this study, zircons younger than 100 Ma have low Th/U ratios (<0.3), except for one grain with a higher ratio (1.46), resembling the Th/U signature of metamorphic zircons (Figure 7c). Additionally, in the $^{206}Pb/^{238}U$ vs. Th/U diagram, only zircons younger than

100 Ma exhibit positively correlated Th/U ratios and U-Pb ages (Figure 7d). Given that these zircons often form rims around zircons aged 500–200 Ma, we interpret them as metamorphic recrystallized zircons.

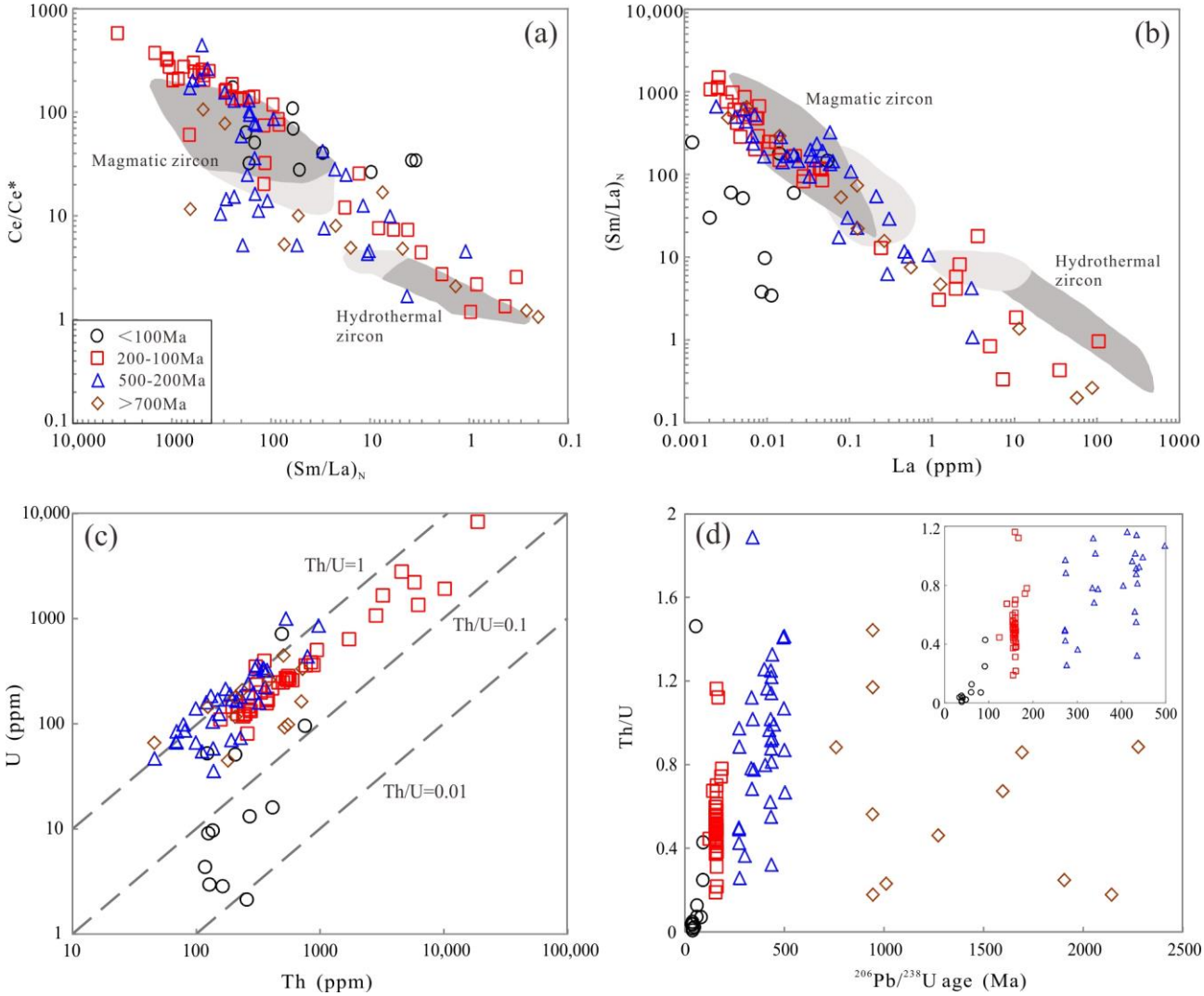

Figure 7. (**a**) Zircon $(Sm/La)_N$ vs. Ce/Ce* diagram; (**b**) zircon La vs. $(Sm/La)_N$ diagram; (**c**) zircon Th vs. U diagram; and (**d**) zircon $^{206}Pb/^{238}U$ age vs. Th/U diagram. Fields in Figure a-b are after [37].

Metamorphic recrystallized zircons also tend to have lower REE contents than magmatic zircons, with gently rising HREE patterns, weak Ce anomalies, and weak or absent Eu anomalies. This REE depletion results from the expulsion of REEs from the zircon lattice during recrystallization [37]. In this study, zircons younger than 100 Ma show much lower REE, P, Th, and Y contents compared to magmatic zircons, further supporting their interpretation as metamorphic recrystallized zircons (Figure 8).

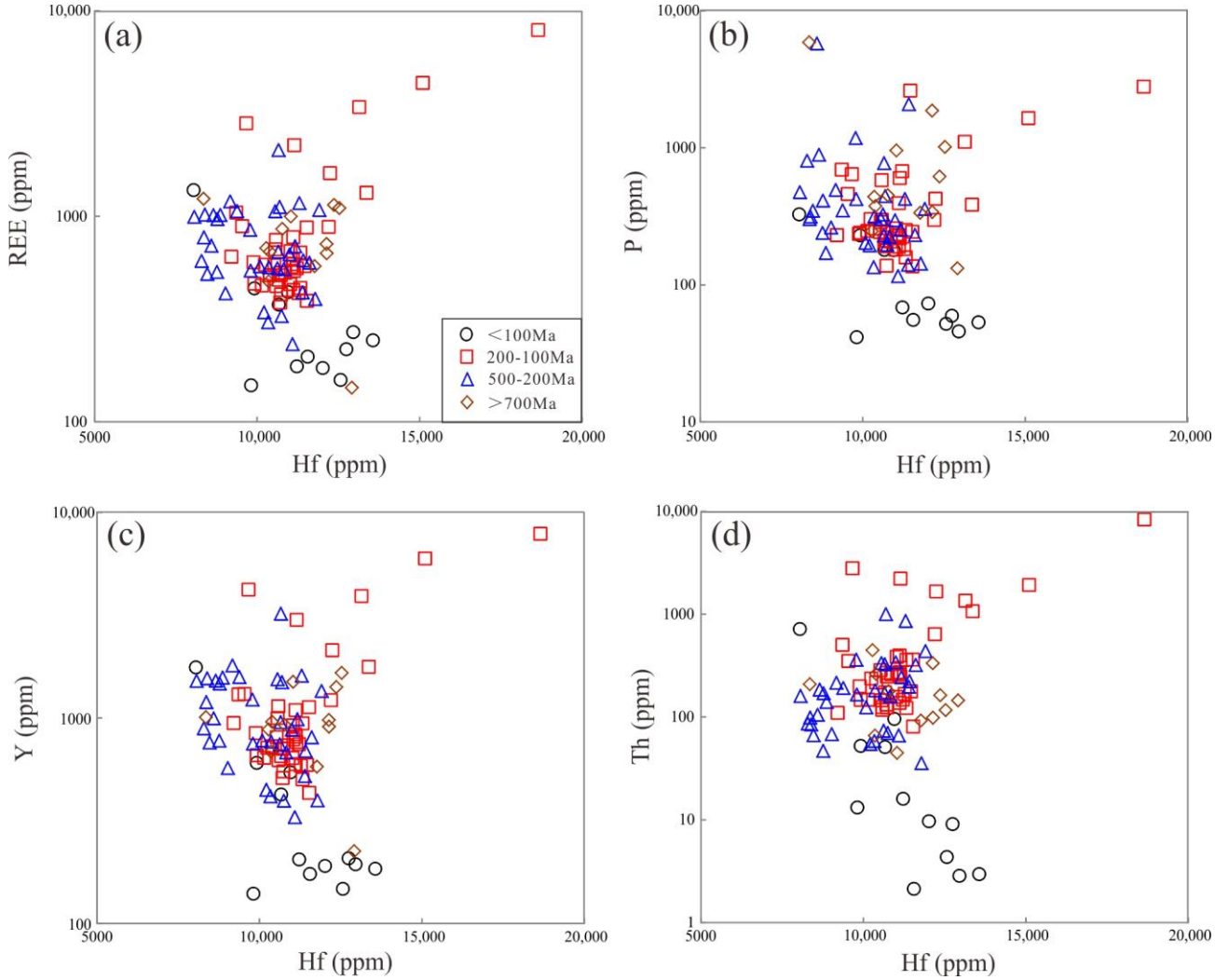

Figure 8. (**a**) Zircon HREE vs. REE diagram; (**b**) zircon Hf vs. P diagram; (**c**) zircon Hf vs. Y diagram; and (**d**) zircon Hf vs. Th diagram.

Overall, this study identifies a portion of zircon grains as hydrothermal, having undergone metamictization and fluid alteration, a portion as metamorphic recrystallized zircon grains or domains, and most as magmatic zircons. Among the magmatic zircons, those aged 170–150 Ma represent original magmatic zircons crystallized in the Laiziling and Jianfengling A-type granites. Zircons older than 170 Ma are interpreted as inherited zircons, and their origins are discussed below.

5.2. Zircon Host Rock Discrimination

Excluding hydrothermal and metamorphic zircons, the remaining zircons are magmatic, either original or inherited, and their trace element compositions can be used to discriminate their host rocks. Incompatible elements are particularly useful for this purpose, as these elements tend to be enriched in more evolved magmas, with zircons from acidic magmas containing higher concentrations of these elements than zircons from basic magmas [47]. Additionally, zircons from magmas with higher oxygen fugacity and evolutionary degrees tend to exhibit lower Eu/Eu^* and Ce/Ce^* ratios [48,49].

In U vs. Y, Eu/Eu* vs. Ce/Ce*, (Yb/Sm)N vs. Y, Nb/Ta vs. Y, Ce/Ce* vs. Y, and Ta vs. Nb discrimination diagrams (Figure 9), zircons aged 200–100 Ma plot in the syenite pegmatite field, indicating intermediate-acidic host rocks. Zircons aged 500–200 Ma and >700 Ma plot in both syenite pegmatite and mafic rock fields, suggesting a variety of host rocks, including intermediate-acidic and mafic lithologies.

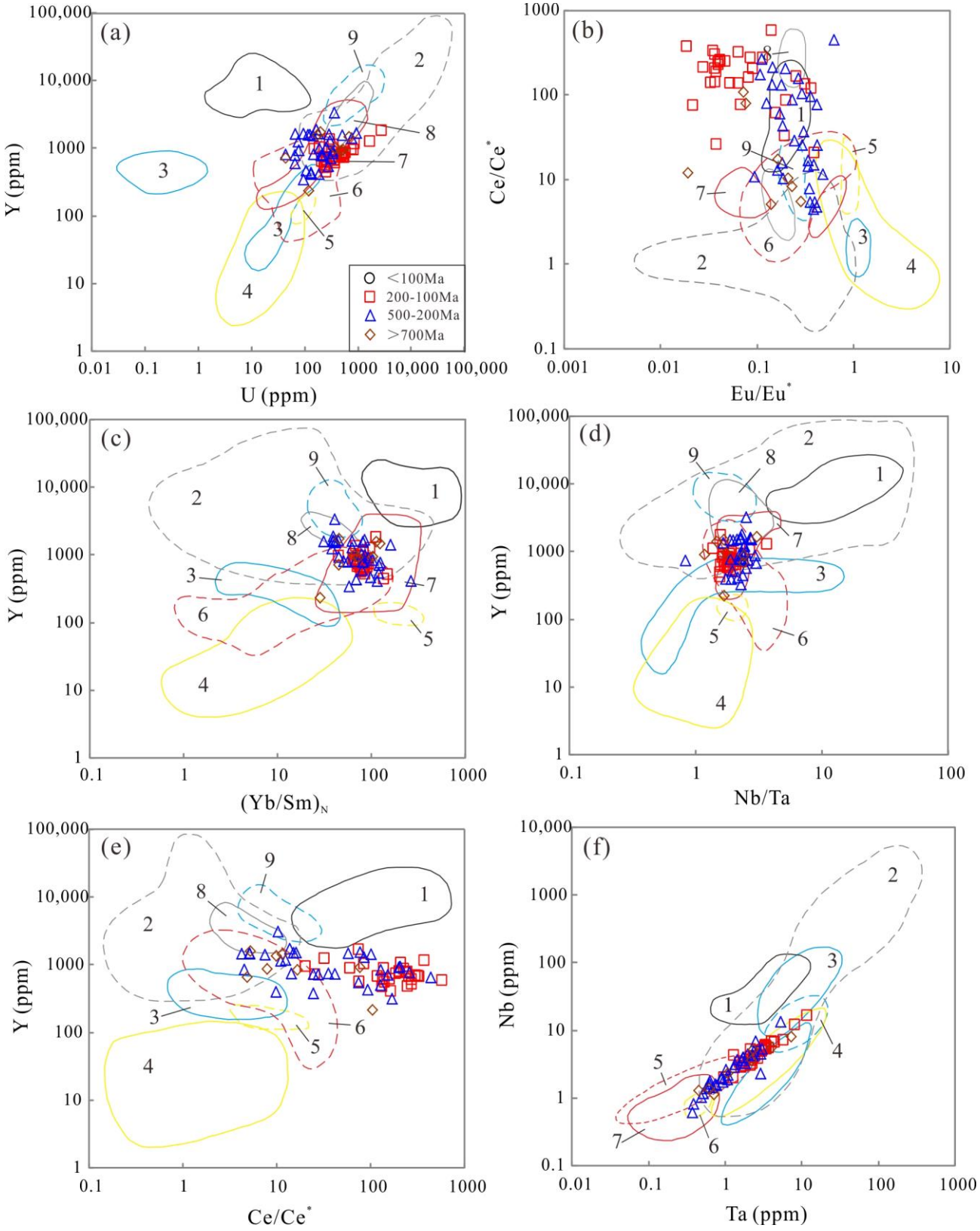

Figure 9. Host rock discrimination diagrams of magmatic zircons (after [47]): (**a**) U vs Y; (**b**) Eu/Eu^* vs Ce/Ce^*; (**c**) $(Yb/Sm)_N$ vs Y; (**d**) Nb/Ta vs Y; (**e**) Ce/Ce^* vs Y; (**f**) Ta vs Nb. The number of the fields represent the following: 1. nepheline syenite and syenite pegmatite; 2. granitoid; 3. carbonatite; 4. kimberlite; 5. syenite; 6. lamproite; 7. mafic rock; 8. syenite pegmatite; and 9. larvikite.

Using classification and regression tree (CART) diagrams [47] (Figure 10), zircons aged 200–100 Ma are most commonly associated with larvikite host rocks, indicating

alkaline, intermediate-acid compositions. Zircons aged 500–200 Ma and >700 Ma are divided into two groups, with one group associated with larvikite and the other with dolerite and carbonatite host rocks, suggesting a mix of alkaline intermediate-acidic and mafic host rocks.

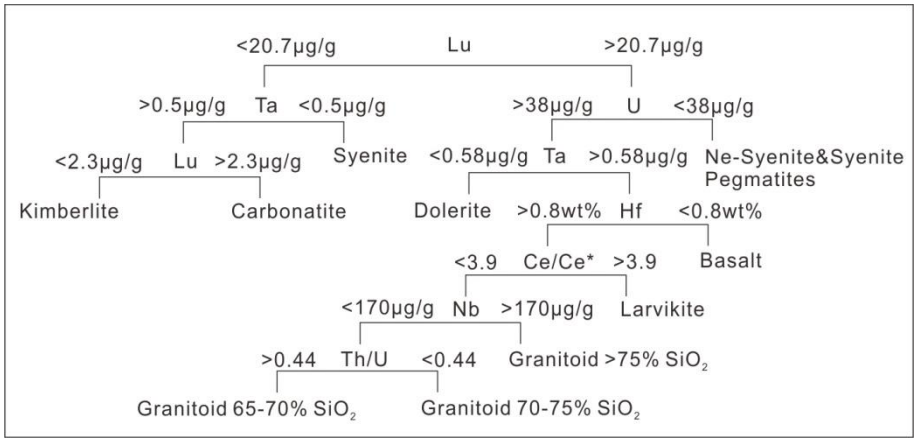

Figure 10. CART tree diagram of zircon host rock discrimination (after [47]).

While zircon trace elements cannot precisely distinguish their exact host rock types, they offer valuable insights into their general composition. Previous studies have discovered that zircons from S-, I-, and A-type granites have different trace element compositions, zircons from I-type granites have lower Pb and higher Th contents than those from S-type granites, and A-type granites have higher Eu/Eu* ratios than I- and S-type granites [34,50,51]. The majority of zircons in the 200–100 Ma age group crystallized in highly evolved granites, as reflected by their A-type granite signature (Figure 11). In contrast, inherited zircons aged 500–200 Ma and >700 Ma, associated with S-type granites and basic rocks, likely formed in earlier tectonic environments.

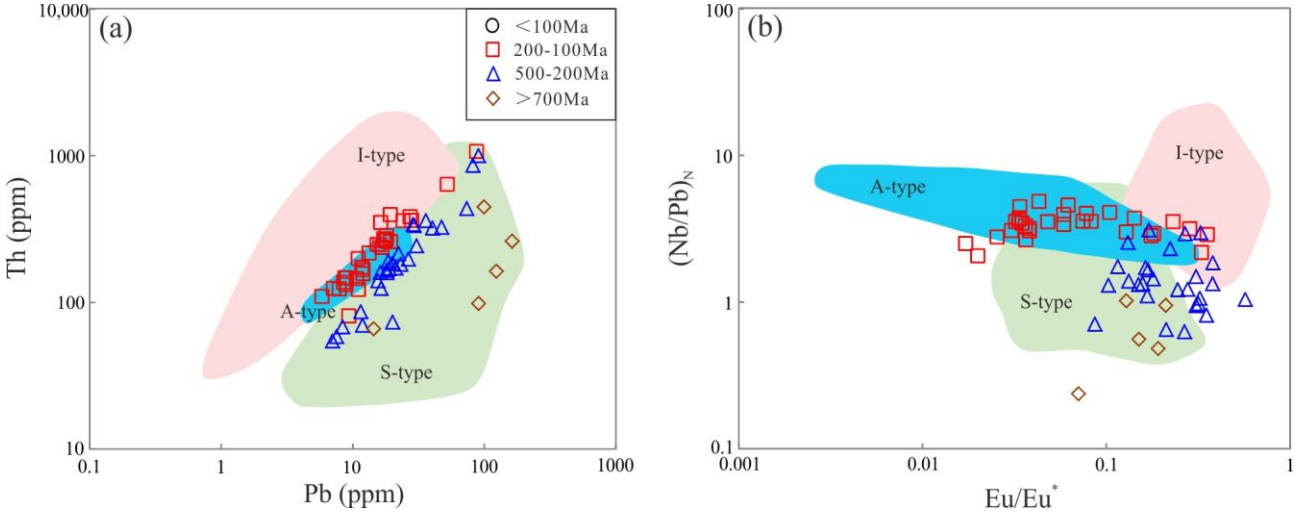

Figure 11. (**a**) Zircon Pb vs. Th diagram; (**b**) zircon Eu/Eu* vs. $(Nb/Pb)_N$ diagram. Fields in figures are after [34].

5.3. Source and Tectonic Settings

Igneous rocks formed in different tectonic environments exhibit distinct geochemical signatures, and the zircons crystallized within these rocks often inherit these characteristics, which can be used to infer the tectonic setting in which they formed. Previous studies have demonstrated that zircon trace element compositions are reliable indicators for discriminating the tectonic environment of their host rocks. Ref. [52] investigated

metamorphic basic rocks from various tectonic settings worldwide and found that zircons crystallized in mid-ocean ridges, volcanic arcs, and within-plate environments display distinct trace element patterns. In this study, discrimination diagrams (Figure 12) show that zircons aged 500–200 Ma and >700 Ma, hosted in basic rocks, plot in the volcanic arc field, suggesting their crystallization occurred in subduction-related volcanic arc settings under compressional tectonics.

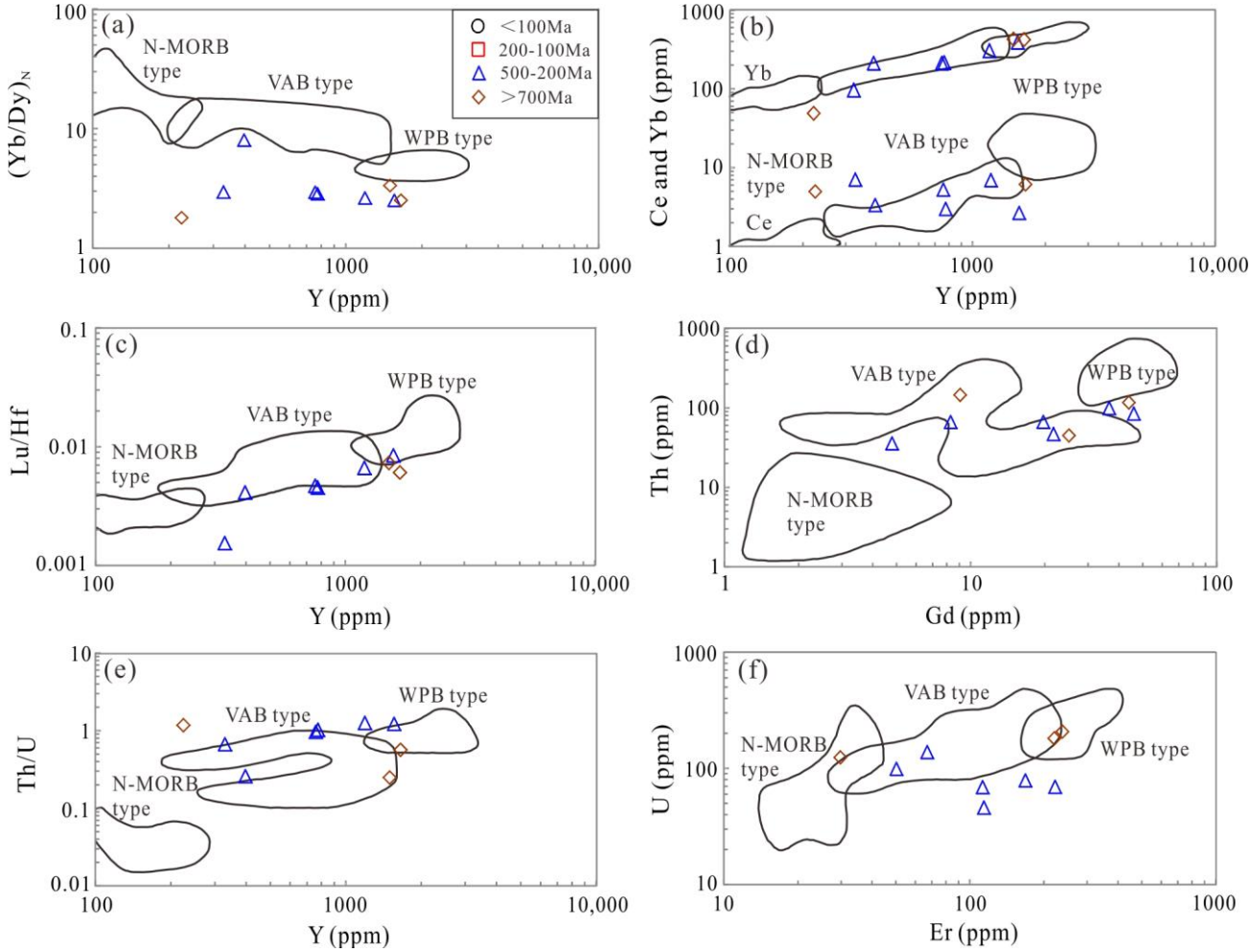

Figure 12. (**a**) Zircon Y vs. $(Yb/Dy)_N$ diagram; (**b**) zircon Y vs. Ce and Y vs. Yb diagram; (**c**) zircon Y vs. Lu/Hf diagram; (**d**) zircon Gd vs. Th diagram; (**e**) zircon Y vs. Th/U diagram; and (**f**) zircon Er vs. U diagram. Fields in figures are after [52]. Abbreviations: N-MORB—normal mid-oceanic ridge basalt; VAB—volcanic arc basalt; WPB—within plate basalt.

Similarly, Ref. [53] proposed a method using zircon trace elements to differentiate between continental and oceanic crust origins. They found that zircons formed in continental crusts are generally more enriched in Th and U compared to those crystallized in oceanic crust, which are depleted in Yb, Y, and Hf. Based on this work, Ref. [54] further refined this classification by associating specific zircon trace element signatures with more detailed tectonic settings, such as continental arcs, continental hotspots, rift valleys, and mid-ocean ridges. They observed that the partitioning of rare earth elements (REEs) and Y in zircons is strongly influenced by the temperature and water content of the magma. For instance, zircons from rift valleys and mid-ocean ridges, which form in high-temperature and water-deficient conditions, tend to be enriched in middle and heavy REEs (MREEs and HREEs) and Y. In contrast, zircons from continental arcs and hotspots, which form in lower-temperature, water-rich environments, are depleted in these elements. In line with these findings, we used Yb-U, Hf-U/Yb, Y-U/Yb, Sm-Gd/Yb, and Yb-Gd/Yb

discrimination diagrams (Figure 13a–e) to analyze the zircons aged 500–200 Ma and >700 Ma in our study. The majority of these zircons, hosted in basic rocks, plot within the continental arc field, reinforcing the interpretation that they crystallized in subduction-related continental arc settings. Ref. [55] further showed that zircons from mid-ocean ridges and oceanic islands have lower Sc/Yb and U/Yb ratios compared to those from continental arcs, while oceanic island zircons tend to have higher Nb/Yb ratios. Although Sc data are not available for the zircons in our study, in the Nb/Yb vs. U/Yb diagram (Figure 13f), the 500–200 Ma and >700 Ma zircons plot within the continental arc field, which is consistent with the previous findings.

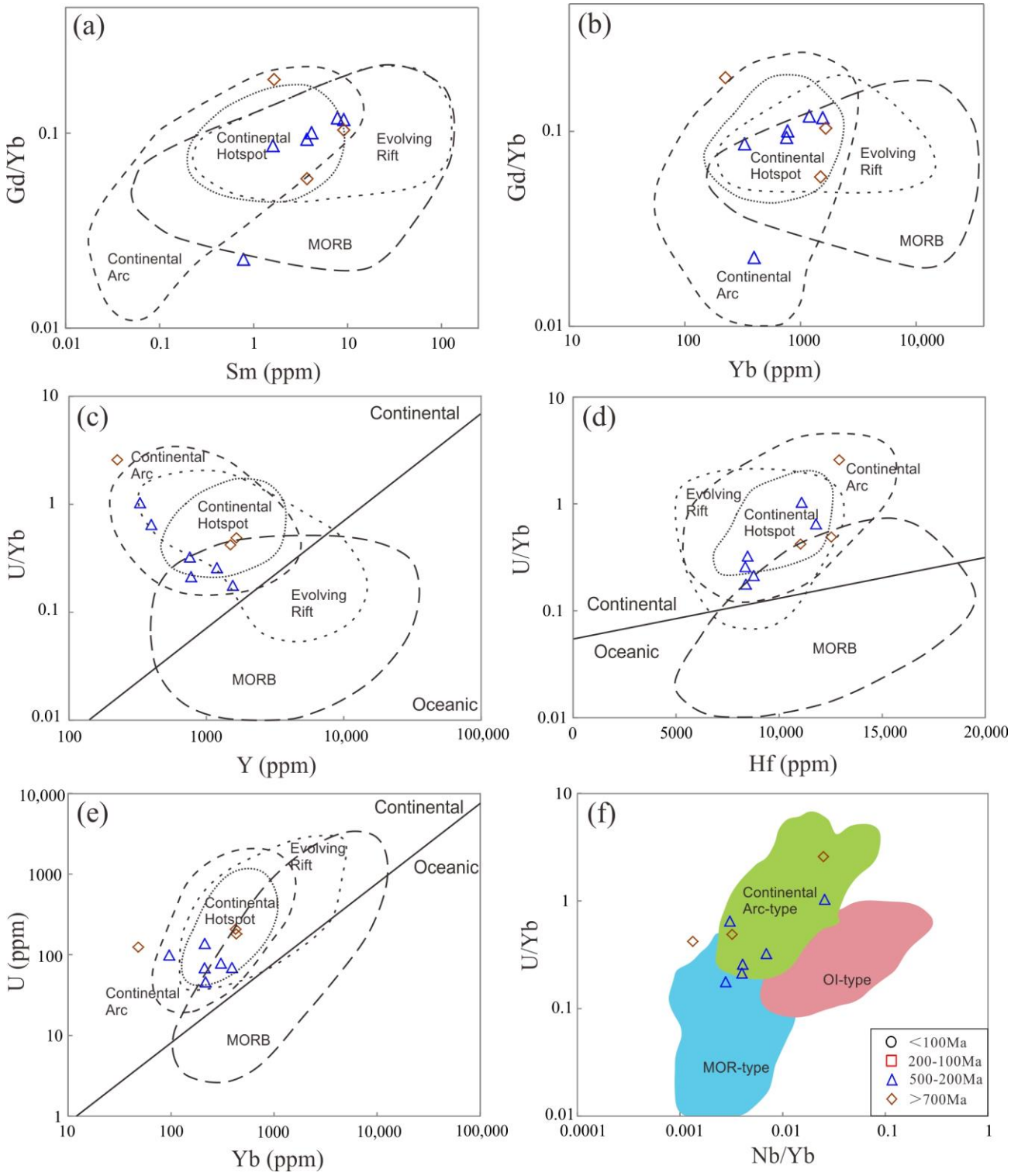

Figure 13. (**a**) Zircon Sm vs. Gd/Yb diagram; (**b**) zircon Yb vs. Gd/Yb diagram; (**c**) zircon Y vs. U/Yb diagram; (**d**) zircon Hf vs. U/Yb diagram; (**e**) zircon Yb vs. U diagram; and (**f**) zircon Nb/Yb vs. U/Yb diagram. Fields in (**a**–**e**) are after [53]; fields in (**f**) are after [54]. Abbreviations: MOR—mid-oceanic ridge; MORB—mid-oceanic ridge basalt; OI—oceanic island.

Among all inherited zircons in this study, excluding those with sporadic dated ages, most are concentrated within five main dated ranges: 950 Ma, 500 Ma, 450 Ma, 350 Ma, and 270 Ma. Zircons dated 350 Ma are predominantly hosted in S-type granites, while those from the other four dated age groups are associated with both S-type granites and basic rocks. Notably, the basic rocks in these cases are also linked to continental arc environments, indicating that the entire Cathaysia Block was under compressional tectonic conditions during these periods (950 Ma, 500 Ma, 450 Ma, 350 Ma, and 270 Ma).

The Hf isotopic composition of the original magmatic zircons, particularly those aged ~150 Ma, show εHf(t) values ranging from −10 to 0, indicating a source in lower crustal granulite-facies igneous rocks. In contrast, the inherited zircons from the five aforementioned age groups, along with some zircons aged ~150 Ma with extremely negative εHf(t) values, predominantly plot in the 2.5–1.6 Ga continental crust growth zone of the Cathaysia Block (Figure 14). This suggests that these zircons are derived from crustal material that was initially separated from the depleted mantle reservoir during the Paleoproterozoic Era, further supporting the idea of a long history of crustal reworking and re-melting events in the region.

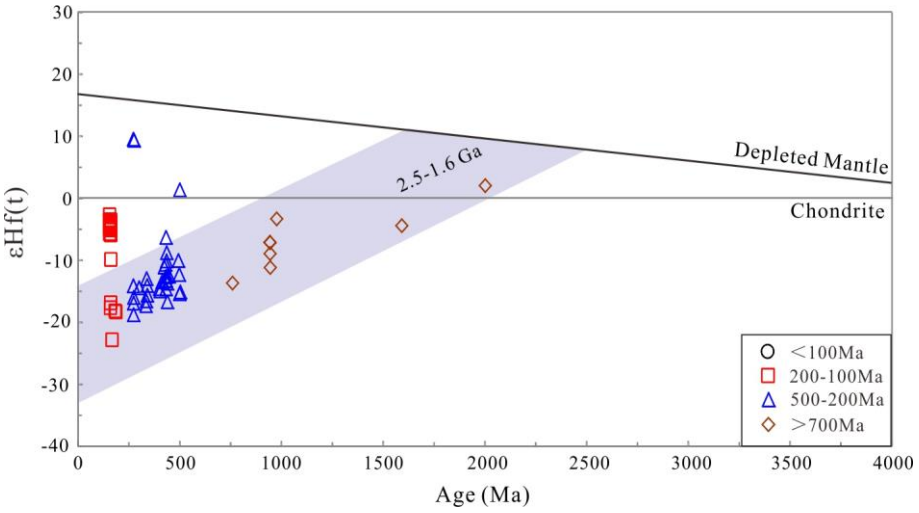

Figure 14. Zircon age vs. **ε**Hf(t) diagram.

5.4. Implications for Tectonic Evolution

As discussed, various crustal materials within the Cathaysia Block were separated from the depleted mantle reservoir during the Paleoproterozoic Era. This indicates that the basement of the Cathaysia Block formed during that period and subsequently underwent multiple re-melting events. These re-melting episodes correspond to several large-scale tectonic events, each associated with distinct magmatic processes. Below, we discuss these tectonic and magmatic events in detail.

During the Neoproterozoic Era, the Cathaysia Block amalgamated with the Yangtze Block along the Jiangnan Orogenic Belt. This period was marked by significant magmatic activity, including the formation of S-type granites, adakitic rocks, and ophiolites [5,56,57]. The oldest sedimentary strata in the Cathaysia Block, represented by the Lengjiaxi and Banxi Groups, show prominent detrital zircon age spectra between 860 and 820 Ma. These strata likely formed in an extensional basin setting during the post-collisional phase following the amalgamation of the Cathaysia and Yangtze Blocks [7]. Ref. [7] propose that this amalgamation occurred in four stages: (1) the initial subduction of the two blocks at

980–880 Ma, forming the Jiangnan Arc, (2) the collision of the Jiangnan Arc with the Cathaysia Block at 880–850 Ma, (3) the collision of the Yangtze Block with the Jiangnan Arc at 860–800 Ma, and (4) a transition to an extensional environment at 800–760 Ma. Based on this model, we suggest that the ~950 Ma zircons identified in this study likely originated from S-type granites formed during the subduction phase of the Cathaysia-Yangtze collision.

The South China Block transitioned into an intraplate tectonic regime during the Paleozoic Era. However, a significant intracontinental orogenic event occurred in the mid-Paleozoic Era, driving widespread magmatism [58–60]. According to [61], this orogeny unfolded in four stages: (1) prior to 460 Ma, the region experienced post-Neoproterozoic extension, leading to the formation of intracontinental basins under stable sedimentary conditions; (2) from 460 to 433 Ma, crustal thickening initiated the orogeny, producing abundant syn-collisional S-type granites; (3) from 443 to 419 Ma, the interaction between the thickened lower crust, the lithospheric mantle, and the asthenosphere triggered larger-scale magmatism, forming granites enriched with mantle-derived material; and (4) from 419 to 380 Ma, mantle input diminished, resulting in more subdued magmatic activity. The ~450 Ma zircons in this study likely crystallized in S-type granites formed during this intracontinental orogeny. In contrast, magmatic activity associated with the 500 Ma, 350 Ma, and 270 Ma zircon populations was more sporadic. The lower abundance of zircons from these ages, compared to the 450 Ma zircons, further supports the interpretation of these events as isolated magmatic episodes rather than widespread tectonic or magmatic phenomena.

The Mesozoic Era was characterized by extensive magmatic activity across the South China Block, leading to the development of prominent granitic provinces and metallogenic belts [62,63]. The most significant magmatic events occurred around 220 Ma, 175–150 Ma, and 135–80 Ma. The 220 Ma magmatism is linked to the collision and amalgamation of various terranes with the South China Block, while the 175–150 Ma and 135–80 Ma magmatic events are associated with the subduction of the Paleo-Pacific plate (Mao et al., 2013). The large-scale A_2-type granites found in the Nanling Range formed in an extensional intraplate environment triggered by the subduction and subsequent exhumation of the Paleo-Pacific slab [64]. The abundance of zircons aged 170–150 Ma in this study represents original magmatic zircons crystallized in A-type granites during this period. Some of these zircons display highly negative $\varepsilon Hf(t)$ values, suggesting that they were derived from more evolved crustal sources within their magmatic origins.

The cessation of Paleo-Pacific subduction led to a series of magmatic and metamorphic processes that migrated from inland to coastal areas of the South China Block [65]. As subduction slowed and eventually halted, these magmatic and metamorphic processes ceased, occurring earlier inland and persisting longer in coastal regions. Ref. [65] suggest that the South China Block continued to experience extensional metamorphic events between the Cretaceous and Tertiary periods, resulting in the formation of numerous uranium deposits, with metallogenesis occurring between 27 and 90 Ma. Based on this framework, we propose that the zircons in this study with ages <100 Ma are likely related to these late-stage extensional metamorphic processes.

6. Conclusions

A comprehensive study of zircon U-Pb ages, trace elements, and Hf isotopic compositions from Jurassic Laiziling and Jianfengling A-type granites has yielded several important findings:

1. Based on U-Pb dating, zircons from the Laiziling and Jianfengling granites can be divided into four distinct age groups, <100 Ma, 200–100 Ma, 500–200 Ma, and >700 Ma, representing a range of geological events and processes.
2. Trace element analysis revealed that the zircons aged <100 Ma are predominantly metamorphic recrystallized zircons. Those aged 200–100 Ma are primarily magmatic

zircons formed during the crystallization of the Laiziling and Jianfengling A-type granites. Zircons aged 500–200 Ma and >700 Ma are inherited zircons, originally crystallized in S-type granites and basic rocks that formed in subduction-compression tectonic environments.

3. The zircons in this study correspond to multiple significant tectonic events in the South China Block. Zircons older than 700 Ma crystallized in S-type granites and basic rocks formed during the Neoproterozoic amalgamation of the Yangtze and Cathaysia Blocks. Zircons aged 500–200 Ma were also crystallized in S-type granites and basic rocks during the Middle Paleozoic intracontinental orogenic event. Zircons aged 200–100 Ma represent magmatic activity linked to the subduction and exhumation of the Paleo-Pacific slab, forming the Laiziling and Jianfengling A-type granites. Zircons younger than 100 Ma indicate extensional metamorphic events from the Cretaceous to the Tertiary Eras.
4. The Hf isotopic compositions of inherited zircons (500–200 Ma and >700 Ma) plot within the 1.6–2.5 Ga crustal evolution zone, suggesting that these zircons were derived from juvenile materials that originally separated from the depleted mantle reservoir during the Paleoproterozoic Era. This provides evidence for multiple re-melting events in the Paleoproterozoic basement of the Cathaysia Block.

Supplementary Materials: The following supporting information can be downloaded at https://www.mdpi.com/article/10.3390/min14121247/s1, Supplementary Table S1: Collected coordinate of granite samples from the Laiziling and Jianfengling plutons. Supplementary Table S2: LA-ICP-MS U-Pb dating results of zircons from the Laiziling and Jianfengling granites. Supplementary Table S3: Trace element compositions of concordant zircons from the Laiziling and Jianfengling granites. Supplementary Table S4: Hf isotopic compositions of concordant zircons from the Laiziling and Jianfengling granites.

Author Contributions: Conceptualization, W.X.; methodology,c software, M.S.; validation, M.S.F.; formal analysis, W.X.; investigation, W.X., I.V.S. and M.S.; resources, W.X., I.V.S. and M.S.; data curation, F.Z., C.Z. and F.X.; writing—original draft, W.X.; preparation, W.X.; writing—review and editing, F.Z., C.Z., F.X., M.S.F. and M.S.; visualization, W.X.; supervision, W.X., I.V.S., M.S.F., and M.S.; project administration, W.X., I.V.S., M.S.F., and M.S.; funding acquisition, W.X., I.V.S., M.S.F., and M.S. All authors have read and agreed to the published version of the manuscript.

Funding: This research was funded by Researchers Supporting Project Number (RSP2024R249), King Saud University, Riyadh, Saudi Arabia. Additional financial support was provided by the Open Research Fund Program of the Fundamental Science on Radioactive Geology and Exploration Technology Laboratory at East China University of Technology (2022RGET04), the Provincial Natural Science Foundation of Hunan (2023JJ40541), the National Nature Science Foundation of China (41002022) and the Key R&D Program of China (grant no. 2017YFC0602402)

Data Availability Statement: Data are contained within the article and supplementary materials.

Acknowledgments: We gratefully acknowledge the valuable comments and suggestions provided by the anonymous reviewers and the editor, which significantly enhanced the clarity of the manuscript and the interpretation of the data.

Conflicts of Interest: The authors declare no conflicts of interest.

References

1. Shu, X.J.; Wang, X.L.; Sun, T.; Chen, W.F.; Shen, W.Z. Crustal formation in the Nanling Range, South China craton: Hf isotope evidence of zircons from Phanerozoic granitoids. *J. Asian Earth Sci.* **2013**, *74*, 210–224.
2. Zhang, S.B.; Zheng, Y.F. Formation and evolution of Precambrian continental lithosphere in South China. *Gondwana Res.* **2013**, *23*, 1243–1260.
3. Li, X.H.; Li, Z.X.; Li, W.X. Detrital zircon U-Pb age and Hf isotope constrains on the generation and reworking of Precambrian continental crust in the Cathaysia Block, South China: A synthesis. *Gondwana Res.* **2014**, *25*, 1202–1215.
4. Zhao, G. Jiangnan Orogen in South China: Developing from divergent double subduction. *Gondwana Res.* **2015**, *27*, 1173–1180.
5. Xia, Y.; Xu, X.S.; Niu, Y.L.; Liu, L. Neoproterozoic amalgamation between Yangtze and Cathaysia blocks: The magmatism in various tectonic settings and continent-arc-continent collision. *Precambrian Res.* **2018**, *309*, 56–87.
6. Zhao, G.C.; Cawood, P.A. Precambrian geology of China. *Precambrian Res.* **2012**, *222–223*, 12–54.

7. Wang, J.; Shu, L.; Santosh, M. U-Pb and Lu-Hf isotopes of detrital zircon grains from Neoproterozoic sedimentary rocks in the central Jiangnan Orogen, South China: Implications for Precambrian crustal evolution. *Precambrian Res.* **2017**, *294*, 175–188.
8. Yu, J.H.; Wang, L.J.; O'Reilly, S.Y.; Griffin, W.L.; Zhang, M.; Li, C.Z.; Shu, L.S. A Paleoproterozoic orogeny recorded in a long-lived cratonic remnant (Wuyishan terrane), eastern Cathaysia Block, China. *Precambrian Res.* **2009**, *174*, 347–363.
9. Yu, J.H.; O'Reilly, S.Y.; Zhou, M.F.; Griffin, W.L.; Wang, L.J. U-Pb geochronology and Hf-Nd isotopic geochemistry of the Badu Complex, Southeastern China: Implications for the Precambrian crustal evolution and paleogeography of the Cathaysia Block. *Precambrian Res.* **2012**, *222–223*, 424–449.
10. Zhao, L.; Zhou, X.W.; Zhai, M.G.; Santosh, M.; Ma, X.D.; Shan, H.X.; Cui, X.H. Paleoproterozoic tectonic transition from collision to extension in the eastern Cathaysia Block, South China: Evidence from geochemistry, zircon U-Pb geochronology and Nd-Hf isotopes of a granite-charnockite suite in southwestern Zhejiang. *Lithos* **2014**, *184–187*, 259–280.
11. Yu, J.H.; O'Reilly, S.Y.; Wang, L.J.; Griffin, W.L.; Zhou, M.F.; Zhang, M.; Shu, L.S. Components and episodic growth of Precambrian crust in the Cathaysia Block, South China: Evidence from U-Pb ages and Hf isotopes of zircons in Neoproterozoic sediments. *Precambrian Res.* **2010**, *181*, 97–114.
12. Li, H.; Wu, J.; Evans, N.J.; Jiang, W.; Zhou, Z. Zircon geochronology and geochemistry of the Xianghualing A-type granitic rocks: Insights into multi-stage Sn-polymetallic mineralization in South China. *Lithos* **2018**, *312–313*, 1–20.
13. Yuan, D.; Tang, X.; Shi, X.; Bao, J.; Liu, K.; Fan, J.; Guo, Y. Zircon Geochronology and Geochemistry of the Taohualing Pluton in Northern Dabieshan and Their Tectonic Implications. *J. Xinyang Norm. Univ. (Nat. Sci. Ed.)* **2022**, *35*, 97–102. (In Chinese with English abstract)
14. Yao, J.; Shu, L.; Santosh, M. Detrital zircon U-Pb geochronology, Hf-isotopes and geochemistry-New clues for the Precambrian crustal evolution of Cathaysia Block, South China. *Gondwana Res.* **2011**, *20*, 553–567.
15. Li, S.L.; Lai, J.Q.; Xiao, W.Z.; Belousova, E.A.; Rushmer, T.; Zhang, L.J.; Ou, Q.; Liu, C.Y. Crustal growth event in the Cathaysia Block at 2.5 Ga: Evidence from chronology and geochemistry of captured zircons in Jurassic acidic dykes. *Geol. Mag.* **2021**, *158*, 567–582.
16. Xiao, W.; Liu, C.; Tan, K.; Duan, X.; Shi, K.; Sui, Q.; Feng, P.; Sami, M.; Ahmed, M.S.; Zi, F. Two Distinct Fractional Crystallization Mechanisms of A-Type Granites in the Nanling Range, South China: A Case Study of the Jiuyishan Complex Massif and Xianghualing Intrusive Stocks. *Minerals* **2023**, *13*, 605.
17. Li, Z.; Lei, X.; Han, Z.; Qiao, Q.; Yan, J. Geomorphic Characteristics of the Tongbai-Dabie Mountain Area and Their Indicative Significance. *J. Xinyang Norm. Univ. (Nat. Sci. Ed.)* **2023**, *36*, 523–527. (In Chinese with English abstract)
18. Mao, J.W.; Xie, G.Q.; Guo, C.L.; Chen, Y.C. Large-scale tungsten-tin mineralization in the Nanling region, South China: Metallogenic ages and corresponding geodyamic processes. *Acta Petrol. Sin.* **2007**, *23*, 2329–2338 (In Chinese with English abstract)
19. Xie, L.; Wang, Z.; Wang, R.; Zhu, J.; Che, X.; Gao, J.; Zhao, X. Mineralogical constraints on the genesis of W-Nb-Ta mineralization in the Laiziling granite (Xianghualing district, south China). *Ore Geol. Rev.* **2018**, *95*, 695–712.
20. Diao, X.; Wu, M.; Zhang, D.; Liu, J. Textural features and chemical evolution of Ta-Nb-W-Sn oxides in the Jianfengling Deposit, South China. *Ore Geol. Rev.* **2022**, *142*, 104690.
21. Liu, Y.; Gao, S.; Hu, Z.; Gao, C.; Zong, K.; Wang, D. Continental and oceanic crust recycling-induced melt-peridotite interactions in the trans-North china orogen: U-Pb dating, Hf isotopes and trace elements in zircons from mantle xenoliths. *J. Petrol.* **2010**, *51*, 537–571.
22. Hu, Z.; Liu, Y.; Chen, L.; Zhou, L.; Li, M.; Zong, K. Contrasting matrix induced elemental fractionation IN NIST SRM and rock glasses during laser ablation ICP-MS analysis at high spatial resolution. *J. Anal. At. Spectrom.* **2011**, *26*, 425–430.
23. Liu, Y.S.; Hu, Z.C.; Zong, K.Q.; Gao, C.G.; Gao, S.; Xu, J. Reappraisement and refinement of zircon U-Pb isotope and trace element analyses by LA-ICP-MS. *Sci. Bull.* **2010**, *55*, 1535–1546.
24. Andersen, T. Correction of common lead in U-Pb analyses that do not report 204Pb. *Chem. Geol.* **2002**, *192*, 59–79.
25. Ludwig, K.R. *User's Manual for Isoplot 3.00, A Geochronological Toolkit for Microsoft Excel*; Berkeley Geo-chronology Center: Berkeley, CA, USA, 2003; Special Publication no. 4.
26. Sun, S.S.; and Mcdonough, W.F. Chemical and isotopic systematics of oceanic basalts: Implications for mantle composition and processes. *Geol. Soc. Lond. Spec. Publ.* **1989**, *42*, 313–345.
27. Wu, Y.B.; Zheng, Y.F. Research on the zircon genetic mineralogy and constrains of the its U-Pb ages. *Chin. Sci. Bull.* **2004**, *49*, 1589–1604. (In Chinese)
28. Xiao, W.; Lai, J.; Jeffrey, M.; Mao, X.; Chen, Y.; Ou, Q.; Xie, F.; Zeng, R. Tectonic affinity and evolution of the Alxa Block during the Neoproterozoic: Constraints from zircon U-Pb. dating, trace elements, and Hf isotopic composition. *Geol. J.* **2018**, *54*, 3700–3719.
29. Zhang, C.; Li, C.; Jiang, J.; Qin, H.; Liu, M.; Zhou, H.; Shi, X. Geochemical Characteristics of REE and Trace Elements Compositions and Geological Significance of Longhuo Gold-antimony Deposit in Guangxi. *J. Xinyang Norm. Univ. (Nat. Sci. Ed.)* **2022**, *35*, 103–107. (In Chinese with English abstract)
30. Zhang, C.; Liu, Y.; Yao, Y.; Yan, Y.; Shi, X. Characteristics of Mineralogy and Its Implications for Ore-forming Mechanism of the Apalieke Cu-polymetallic Deposit in Xinjiang. *J. Xinyang Norm. Univ. (Nat. Sci. Ed.)* **2023**, *36*, 76–81. (In Chinese with English abstract)
31. Yang, F.; Santosh, M.; Tsunogae, T.; Tang, L.; Teng, X. Multiple magmatism in an evolving suprasubduction zone mantle wedge: The case of the composite mafic–ultramafic complex of Gaositai, North China Craton. *Lithos* **2017**, *284–285*, 525–544.

32. Tang, X.; Yang, W.; Yan, Y.; Guo, Y.; Zhang, Y.; Yang, L. Characteristics of Trace Elements in Pyrite and Their Implications for the Genesis of Yindongpo Gold Deposit in Henan Province. *J. Xinyang Norm. Univ. (Nat. Sci. Ed.)* **2023**, *36*, 445–450. (In Chinese with English abstract)
33. Zhao, K.D.; Jiang, S.Y.; Ling, H.F.; Palmer, M.R. Reliability of LA-ICP-MS U-Pb dating of zircons with high U concentrations: A case study from the U-bearing Douzhashan Granite in South China. *Chem. Geol.* **2014**, *389*, 110–121.
34. Zhao, Z.D.; Liu, D.; Wang, Q.; Zhu, D.C.; Dong, G.C.; Zhou, S.; Mo, X.X. Zircon trace elements and their use in probing deep processes. *Earth Sci. Front.* **2018**, *25*, 124–135. (In Chinese with English Abstract)
35. Zeng, R.; Allen, B.M.; Mao, X.; Lai, J.; Yan, J.; Wu, J. Whole-rock and zircon evidence for evolution of the Late Jurassic high-Sr/Y Zhoujiapuzi granite, Liaodong Peninsula, North China Craton. *Solid Earth* **2022**, *13*, 1259–1280.
36. Hoskin, P.W.O.; Kinny, P.D.; Wyborn, D.; Chappell, B.W. Identifying accessory mineral saturation during differentiation in granitoid magmas: An integrated approach. *J. Petrol.* **2000**, *41*, 1365–1396.
37. Hoskin, P.W.O. Trac-element composition of hydrothermal zircon and the alteration of Hadean zircon from the Jack Hills, Australia. *Geochim. Cosmochim. Acta* **2005**, *69*, 637–648.
38. Hoskin, P.W.O.; Schaltegger, U. The composition of zircon and igneous and metamorphic petrogenesis. *Rev. Mineral. Geochem.* **2003**, *53*, 27–62.
39. Rollinson, H.R.; Windley, B.F. Selective elemental depletion during metamorphism of Archean granulites, Contrib. *Mineral. Petrol.* **1980**, *72*, 257–263.
40. Nozhkin, A.D.; Turkina, O.M. Radiogeochemistry of the charnokite-granulite complex, Sharyzhalgay Window, Siberian Platform. *Geochem. Int.* **1995**, *32*, 62–78.
41. Keay, S.; Lister, G.; Buick, I. The timing of partial melting, Barrovian metamorphism and granite intrusion in the Naxos metamorphic core complex, Cyclades, Aegean Sea, Greece. *Tectonophysics* **2001**, *342*, 275–312.
42. Rubatto, D.; Gebauer, D. Use of cathodoluminescence for U-Pb zircon dating by IOM Microprobe: Some examples from the western Alps. In *Cathodoluminescence in Geoscience*; Springer: Berlin/Heidelberg, Germany, 2000; pp. 373–400.
43. Vavra, G.; Schmid, R.; Gebauer, D. Internal morphology, habit and U-Th-Pb microanalysis of amphibole to granulite facies zircon: Geochronology of the Ivren Zone (Southern Alps). *Contrib. Mineral. Petrol.* **1999**, *134*, 380–404.
44. Pidgeon, R.T.; Nemchin, A.A.; Hitchen, G.J. Internal structures of zircons from Archaean granites from the Darling Range batholith: Implications for zircon stability and the interpretation of zircon U-Pb ages. *Contrib. Mineral. Petrol.* **1998**, *132*, 288–299.
45. Hoskin, P.W.O.; Black, L.P. Metamorphic zircon formation by solid-state recrystallization of protolith igneous zircon. *J. Metamorph. Geol.* **2000**, *18*, 423–439.
46. Tomaschek, F.; Kennedy, A.K.; Villa, I.M.; Lagos, M.; Ballhaus, C. Zircons from Syros, Cyclades, Greece-recrystallization and mobilization of zircon during high-pressure metamorphism. *J. Petrol.* **2003**, *44*, 1977–2002.
47. Belousova, E.; Griffin, W.; O'Reilly, S.Y.; Fisher, N. Igneous zircon: Trace element composition as an indicator of source rock type. *Contrib. Mineral. Petrol.* **2002**, *143*, 602–622.
48. El-Bialy, M.Z.; Ali, K.A. Zircon trace element geochemical constraints on the evolution of the Ediacaran (600–614Ma) post-collisional Dokhan Volcanics and Younger Granites of SE Sinai, NE Arabian–Nubian Shield. *Chem. Geol.* **2013**, *360–361*, 54–73.
49. Wu, Q.; Cao, J.; Kong, H.; Shao, Y.; Li, H.; Xi, X.; Deng, X. Petrogenesis and tectonic setting of the early Mesozoic Xitian granitic pluton in the middle Qin-Hang Belt, South China: Constraints from zircon U-Pb ages and bulk-rock trace element and Sr-Nd-Pb isotopic compositions. *J. Asian Earth Sci.* **2016**, *128*, 130–148.
50. Wang, Q.; Zhu, D.C.; Zhao, Z.D.; Qi, G.; Zhang, X.Q.; Sui, Q.L.; Hu, Z.C.; Mo, X.X. Magmatic zircons from I-, S- and A-type granitoids in Tibet: Trace element characteristics and their application to detrital zircon provenance study. *J. Asia Earth Sci.* **2012**, *54*, 59–66.
51. Xie, F.; Xiao, W.; Sami, M.; Sanislav, V.I.; Ahmed, S.M.; Zhang, C.; Wang, Y.; Yan, B.; Hu, B.; Li, N.; et al. Tectonic evolution of the Northeastern Paleo-Tethys Ocean during the late Triassic: Insights from depositional environment and provenance of the Xujiahe formation. *Front. Earth Sci.* **2023**, *12*, 1444679.
52. Schultz, B.; Klemd, R.; Brätz, H. Host rock compositional controls on zircon trace element signatures in metabasites from the Austroalpine basement. *Geochim. Cosmochim. Acta* **2006**, *70*, 697–710.
53. Grimes, C.B.; John, B.E.; Kelemen, P.N.; Mazdab, F.K.; Wooden, J.L.; Cheadle, M.J.; Hanghoj, K.; Schwartz, J.J. Trace element chemistry of zircons from oceanic crust: A method for distinguishing detrital zircon provenance. *Geology* **2007**, *35*, 643–646.
54. Carley, T.L.; Miller, C.F.; Wooden, J.L.; Padilla, A.J.; Schmitt, A.K.; Economos, R.C.; Bindeman, I.N.; Jordan, B.T. Iceland is not a magmatic analog for the Hadean: Evidence from the zircon record. *Earth Planet. Sci. Lett.* **2014**, *405*, 85–97.
55. Grimes, C.B.; Wooden, J.L.; Cheadle, M.J.; John, B.E. "Fingerprinting" tectono-magmatic provenance using trace elements in igneous zircon. *Contrib. Mineral. Petrol.* **2015**, *170*, 46.
56. Yao, J.L.; Shu, L.S.; Santosh, M.; Zhao, G. Neoproterozoic arc-related mafic-Ultramafic rocks and syn-collision granite from the western segment of the Jiangnan Orogen, South China: Constraints on the Neoproterozoic assembly of the Yangtze and Cathaysia Blocks. *Precambrian Res.* **2014**, *243*, 39–62.
57. Wang, G.G.; Ni, P.; Yao, J.; Wang, X.L.; Zhao, K.D.; Zhu, R.Z.; Xu, Y.F.; Pan, J.Y.; Li, L.; Zhang, Y.H. The link between subduction-modified lithosphere and the giant Dexing porphyry copper deposit, South China: Constraints from high-Mg adakitic rocks. *Ore Geol. Rev.* **2015**, *67*, 109–126.

58. Wang, Y.; Zhang, F.; Fan, W.; Zhang, G.; Chen, S.; Cawood, P.A.; Zhang, A. Tectonic setting of the South China Block in the early paleozoic: Resolving intracontinental and ocean closure models from detrital zircon U-Pb geochronology. *Tectonics* **2010**, *29*, 1–16.
59. Faure, M.; Shu, L.S.; Wang, B.; Charvet, J.; Choulet, F.; Monie, P. Intracontinental subduction: A possible mechanism for the early palaeozoic orogen of SE China. *Terra Nova* **2009**, *21*, 360–368.
60. Charvet, J.; Shu, L.S.; Faure, M.; Choulet, F.; Bo, W.; Lu, H.; Breton, N.L. Structural development of the lower Paleozoic belt of South China: Genesis of an intracontinental orogeny. *J. Asian Earth Sci.* **2010**, *39*, 309–330.
61. Ou, Q.; Lai, J.Q.; Carvalho, B.B.; Zi, F.; Kong, H.; Li, B.; Jiang, Z.Q. Different response to middle-Palaeozoic magmatism during intracontinental orogenic processes: Evidence from southeastern South China Block. *Int. Geol. Rev.* **2019**, *61*, 1504–1521.
62. Mao, J.; Cheng, Y.; Chen, M.; Pirajno, F. Major types and time-space distribution of Mesozoic ore deposits in South China and their geodynamic settings. *Miner. Depos.* **2013**, *48*, 267–294.
63. Li, H.; Palinkaš, A.L.; Watanabe, K.; Xi, X.S. Petrogenesis of Jurassic A-type granites associated with Cu-Mo and W-Sn deposits in the central Nanling region, South China: Relation to mantle upwelling and intra-continental extension. *Ore Geol. Rev.* **2018**, *92*, 449–462.
64. Liu, Y.; Lai, J.; Xiao, W.; Jeffrey, M.D.; Du, R.; Li, S.; Liu, C.; Wen, C.; Yu, X. Petrogenesis and mineralization significance of two-stage A-type granites in Jiuyishan, South China: Constraints from whole-rock geochemistry, mineral composition and zircon U-Pb-Hf isotopes. *Acta Geol. Sin. (Engl. Ed.)* **2019**, *93*, 874–900.
65. Hu, R.Z.; Bi, X.W.; Su, W.C.; Peng, J.T.; Li, C.Y. The relationship between uranium metallogenesis and crustal extension during the cretaceous-tertiary in South China. *Earth Sci. Front.* **2008**, *11*, 153–160.